Autofluorescence Lifetime Imaging of Cultivated Cells Using a UV Picosecond Laser Diode

Herbert Schneckenburger,[1,2,3] Michael Wagner,[1] Petra Weber,[1] Wolfgang S.L. Strauss,[2] and Reinhard Sailer[2]

Lifetime images of autofluorescence of cultivated endothelial cells were recorded using a novel picosecond laser diode in the near ultraviolet range (375 nm). In contrast to existing picosecond light sources this wavelength permits efficient excitation of the free and protein bound coenzyme NADH with fluorescence lifetimes of 0.4–0.5 ns and 2.0–2.5 ns, respectively. The effective fluorescence lifetime τ_{eff} (depending on both lifetimes) was homogenously distributed over the cells with some shortening in the perinuclear region, possibly close to mitochondria. A slight decrease of τ_{eff} was observed after inhibition of the mitochondrial respiratory chain, whereas a slight increase was observed after inhibition of the glycolytic pathway, thus indicating variations of the ratio of free and protein bound NADH. Although present applications are still limited by their low pulse energy (≤ 5 pJ), uv picosecond laser diodes have a large potential in high resolution fluorescence microscopy and fluorescence lifetime endoscopy.

KEY WORDS: Autofluorescence; FLIM; NADH; picosecond uv laser diode.

INTRODUCTION

In recent years autofluorescence has been used increasingly for diagnosis of cells and tissues, e.g. for measuring mitochondrial malfunction [1] or hypoxia [2,3] as well as for tumour detection [4–9]. In addition to the extracellular fluorophores collagen and elastin [10], autofluorescence has been related to the coenzyme nicotinamid adenine dinucleotide (in its reduced form, NADH) as well as to flavin molecules when excited in the near ultraviolet range [11,12]. So far, free NADH and protein bound NADH have been distinguished, the first species (together with nicotinamid adenine dinucleotide phosphate, NADPH) being mainly localized in the cytoplasm and the second species within mitochondria [13]. Due to its higher fluorescence quantum yield [14] mitochondrial NADH has been reported to be the dominating component. After inhibition of the mitochondrial respiratory chain [1,15] or deprivation of oxygen [16] a considerable increase of both, protein bound and free NADH was detected.

Fluorescence spectra of free NADH, protein bound NADH and flavins with emission maxima around 440, 470, and 520 nm are overlapping [12,17]. However, it has been shown previously that these components can be distinguished on the basis of their fluorescence lifetimes of about 0.5, 2.5, and 5–6 ns, respectively [15]. First fluorescence lifetime images of free NADH in solution as well as NADH bound to enzymes have been reported about 10 years ago [18]. In the meantime, time-resolved detection methods have been used by several groups [8,17,19]. However, only in a few cases autofluorescence lifetime imaging of cells or tissues became possible by using either a picosecond laser diode (at 405 nm) together with a highly sensitive camera system [20] or a tunable femtosecond titanium:sapphire laser (750–850 nm) in combination

with a multiphoton scanning microscope [19,21]). Very little NADH (absorption maximum around 350 nm) was excited in the first case, whereas a rather complex (and expensive) optical alignment had to be used in the second case.

For the present investigations a novel picosecond laser diode at 375 nm was integrated in a fluorescence lifetime imaging (FLIM) equipment [22] using single mode fiber optics, an upright fluorescence microscope and a time-gated image intensifying camera with a time resolution of 200 ps. After appropriate adjustment this system permitted reliable and continuous detection of cellular autofluorescence including free and protein bound NADH. Fluorescence was recorded using inhibitors of either the mitochondrial respiratory chain or of the glycolytic pathway, and compared with control cells without inhibitor.

MATERIALS AND METHODS

BKEz-7 endothelial cells from calf aorta [23] were cultivated in RPMI 1640 medium supplemented with 10% fetal calf serum (FCS), glutamine and antibiotics (penicillin, streptomycin) at 37°C and 5% CO_2. For microscopic experiments 150 cells mm^{-2} were seeded on glass slides and grown for 48 hr prior to incubation for 10 min with either rotenone (5 μM in culture medium) or deoxyglucose (10 mM in culture medium). Rotenone is a well-known inhibitor of the first enzyme complex of the mitochondrial respiratory chain [24], whereas deoxyglucose inhibits the glycolytic pathway. After phosphorylation by the enzyme hexokinase, deoxyglucose-6-phosphate cannot be further metabolized. For incubation with rotenone a 1 mM stock solution with ethanol as a solvent was used; therefore the incubation medium contained 0.5 % ethanol. For maintaining identical conditions, 0.5% ethanol was also added to the medium containing deoxyglucose as well as to the medium of control cells without inhibitor. After incubation cells were rinsed with Earl's Balanced Salt Solution (EBSS) and covered with a glass slide prior to microscopic measurements.

Since NADH oxidation is related to the formation of ATP as a final step of the respiratory chain, the intracellular ATP content was measured for control cells as well as for cells incubated with either rotenone (5 μM, 10 min) or deoxyglucose (10 mM, 10 min). Cells were seeded in 4-well-plates (Nunc, Wiesbaden, Germany) at a density of 150 cells mm^{-2}. After 48 hr, cells were incubated, rinsed with phosphate buffered saline (PBS), and ATP was extracted with 200 μL ethanol (96%) per well. After 5 min, the extract was diluted with a buffer solution (100 mM TRIS, 4 mM EDTA, pH 7.8). ATP was measured

luminometrically using a commercially available kit (ATP bioluminescence assay kit CLS II, Boehringer Mannheim, Germany) and a multiplate luminometer (Lucy 1, Anthos Labtec Intruments, Salzburg, Austria).

For fluorescence measurements a microscope (Axioplan 1, Carl Zeiss Jena, Germany) was equipped with a custom-made dark field condensor for illumination by picosecond pulses of a 375 nm laser diode (LDH 375 with driver PDL 800-B, Picoquant, Berlin, Germany; pulse duration: 70 ps, repetition rate: 40 MHz, average power: $\leq$200 μW) using a single mode fiber system (Point Source, kineFlex-p-3-S-395, Southampton, USA), as depicted in Fig. 1. Due to attenuation by the fiber and its collimating optics the average light power in the plane of the sample was limited to 6 μW. Fluorescence was collected using a high aperture oil immersion objective lens (Plan Neofluar 40 × 1.30). A polychromator and an image intensifying system (IMD D4562, Hamamatsu Photonics, Ichino-Cho, Japan) fixed on top of the microscope (not shown in Fig. 1) was used to detect emission spectra before and after each measurement to ensure that neither photobleaching nor any other modification of the sample occurred. Fluorescence images were recorded using an image intensifying camera system (Picostar HR 12 image intensifier coupled to a cooled ICCD camera; LaVision, Göttingen, Germany) with 640 × 480 pixels and 2 × 2 binning in each case. The image intensifier was operated either in the continuous wave (cw) mode or in the time-gated mode with time gates set at 0.3–1.3 ns (A) or 1.3–2.3 ns (B) after the laser pulse, as depicted in Fig. 2. The accumulation time was 1 s for the cw image and 10 s for the time-gated images. The effective fluorescence lifetime τ_{eff} was determined from the intensities I_A and I_B measured within the two time gates according to the relation [25]

$$\tau_{\text{eff}} = \Delta t / \ln(I_A/I_B), \quad (1)$$

with Δt corresponding to the time interval of 1 ns between the two gates. τ_{eff} could be displayed either as an image or as a histogram. For the comparison of cells after inhibition of either the mitochondrial respiratory chain or the glycolytic pathway with untreated control cells, an average of 5 lifetime histograms was calculated in each case. In addition to the fluorescence intensity and lifetime images, decay kinetics were recorded by shifting a 200 ps time gate in multiple steps over a time scale of 10 ns, and evaluated by non-linear curve fitting using up to 3 exponential components.

RESULTS

After inhibition of the mitochondrial respiratory chain (with rotenone) the intracellular content of ATP was
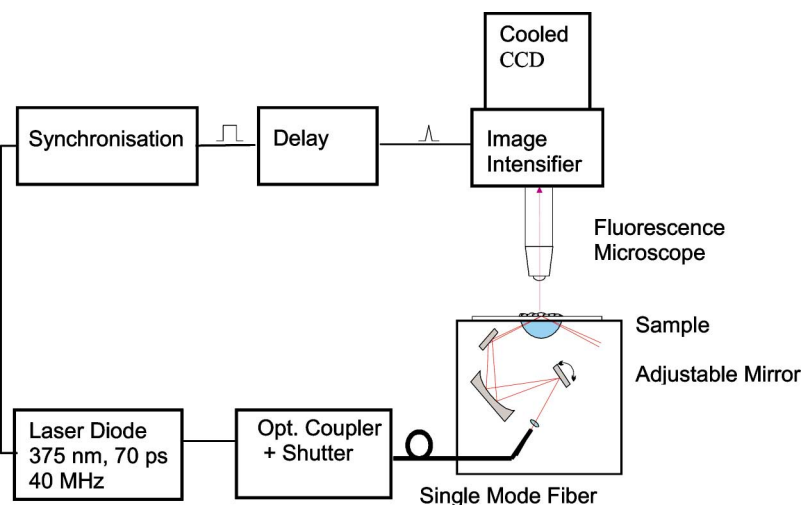
Fig. 1. Fluorescence lifetime imaging equipment using a microscope together with a 375 nm laser diode, a single mode fiber-optic system and a dark field condensor.

reduced to 82% as compared with untreated control cells. In contrast, incubation with deoxyglucose (inhibitor of the glycolytic pathway) did not change the intracellular ATP content. Therefore, only in the case of rotenone cellular energy production was partly compromised.

In all cases, fluorescence spectra recorded prior and after lifetime imaging showed two broad, overlapping bands with maxima at 440–445 nm and 475–480 nm, which are attributed to protein bound and free NADH, respectively. A flavin band around 520 nm (as reported previously [17]) could not be resolved in the present experiments. Fluorescence intensities did not change in the course of individual measurements, i.e. no photobleaching occurred under the present experimental conditions. In addition, spectral shapes were almost the same for all three cell collectives.

A fluorescence decay profile obtained from an object field of about 15 individual cells is depicted in Fig. 2
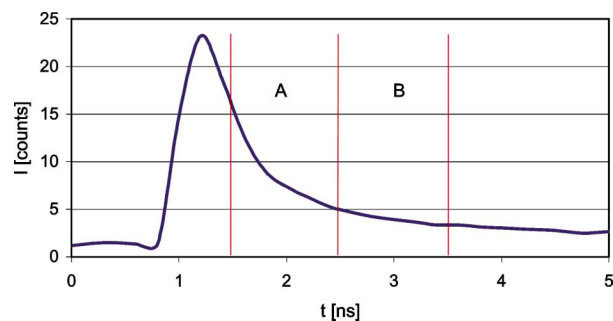

Fig. 2. Decay profile of autofluorescence excited at 375 nm and time gates used for lifetime imaging (A: 0.3–1.3 ns; B: 1.3–2.3 ns after the pulse maximum).

together with the time gates (A,B) used for lifetime imaging. The curve can be fitted by three exponentially decaying components with fluorescence lifetimes of 0.4–0.5 ns, 2.0–2.5 ns and 150–200 ns. The lifetimes of the first two components are comparable to literature values of free NADH (or NADPH) and NADH bound to proteins [13,15], whereas the relatively weak long-lived component is mainly attributed to background luminescence of the optical setup (e.g. glass slides, objective lens). No further fluorescence lifetimes (corresponding e.g. to flavin molecules [15]) could be resolved.

A fluorescence intensity image after cw excitation (a) and a fluorescence lifetime image (b) are depicted in Fig. 3 for cells incubated with 5 μM rotenone. Images of non-incubated control cells as well as cells incubated with 10 mM deoxyglucose are quite similar. The intensity image shows a granular as well as a diffuse pattern all over the cells except from the nuclei, whereas the lifetime image shows a rather homogenous distribution of fluorescence lifetimes. Fluorescent granules of high intensity and slightly reduced lifetime (marked in one case by an arrow) are observed in the perinuclear region.

Figure 4 shows a histogram of effective fluorescence lifetimes for the 3 cell collectives, where each curve is deduced from the average of 5 lifetime images. In all cases, τ_{eff} is distributed between 0.5 ns and about 3 ns with a maximum around 800 ps for non-incubated control cells, 740 ps for cells incubated with rotenone and 860 ps for cells incubated with deoxyglucose. This indicates that the contribution of short-lived fluorophores may be higher after incubation with rotenone and lower after incubation with deoxyglucose in comparison with untreated controls.
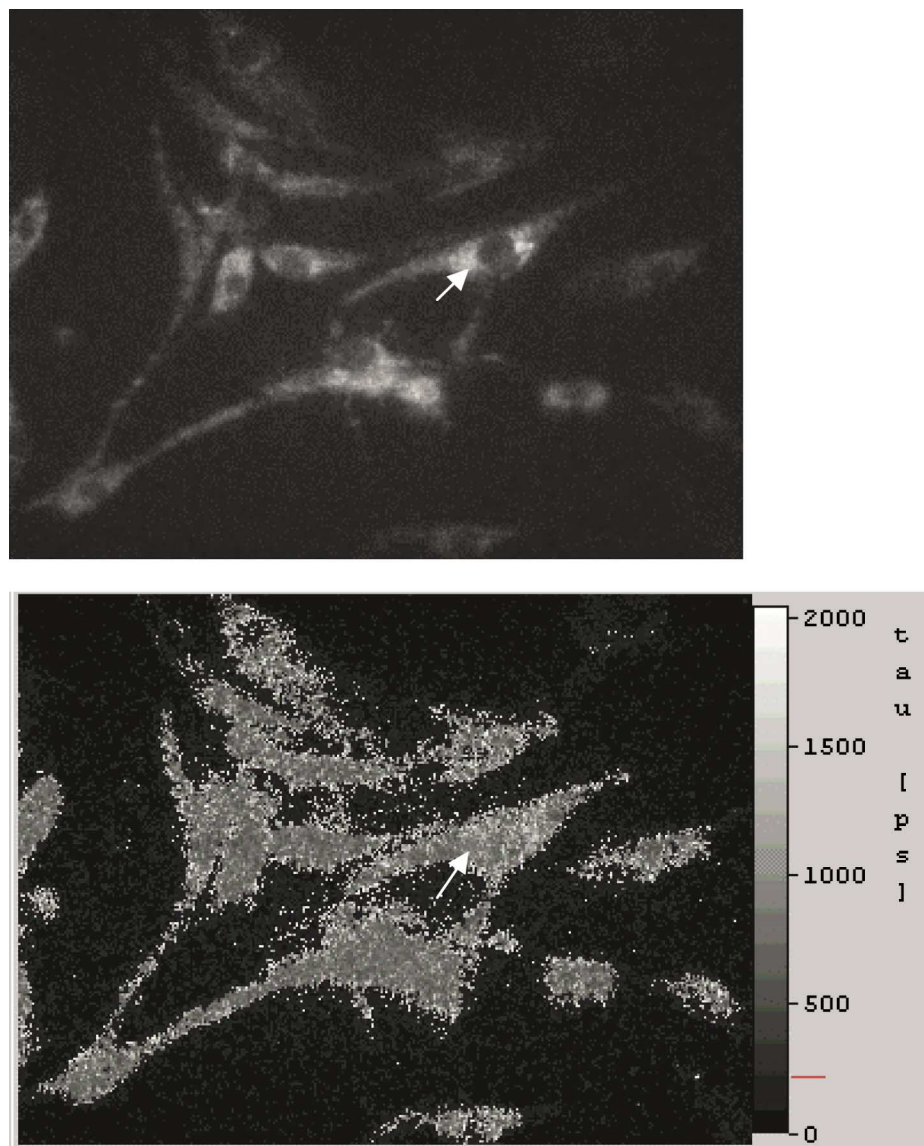
Fig. 3. Intensity (top) and lifetime image (bottom) of autofluorescence of BKEz-7 endothelial cells after incubation with 5 μM rotenone. Excitation wavelength: $\lambda_{ex} = 375$ nm; detection range: $\lambda \geq 420$ nm; image size: 320 μm $\times$ 250 μm. A perinuclear region with a granular fluorescence pattern and reduced lifetime is indicated by an arrow.

DISCUSSION

In spite of the low fluorescence quantum yield of its main components (free NADH: 0.02, protein-bound NADH: 0.1 [14]), intensity and lifetime images of cellular autofluorescence could be recorded using a highly intensifying camera system. In addition to diffuse fluorescence all over the cells, the intensity image shows brigthly fluorescent perinuclear granules, whose distribution resembles that of the mitochondrial marker rhodamine 123 [22]. In the literature about 80% of NADH fluorescence is reported to arise from mitochondria where it is usually bound to proteins [26]. Inhibition of the mitochondrial respiratory chain by various toxins showed an increase of autofluorescence [15], which was partly assigned to free NADH. Now a slight decrease of the effective fluorescence lifetime after incubation with rotenone again indicates an increase of the relative amount of free NADH, whose lifetime (0.4 ns) is considerably shorter than that of bound NADH. Since the granular pattern of fluorescence
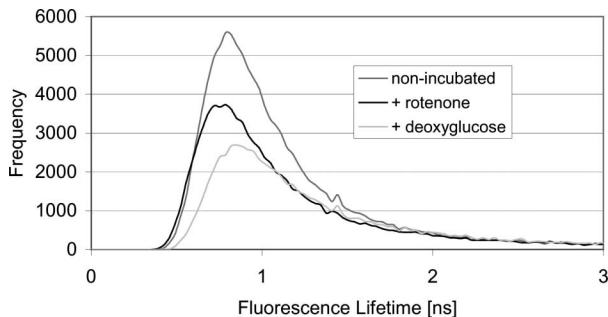
Fig. 4. Histograms of effective fluorescence lifetimes for BKEz-7 endothelial cells incubated with either rotenone or deoxyglucose in comparison with untreated control cells. Histograms were calculated as averages of 5 lifetime images in each case.

intensity is maintained after inhibition of the respiratory chain, and since the effective fluorescence lifetime within some of the granules appears slightly shorter than that of the environment, free NADH seems to be accumulated within or close to the mitochondria. In contrast to incubation with rotenone, it appears that after incubation with deoxyglucose (inhibitor of the glycolytic pathway) the ratio between free and bound NADH is slightly lowered in comparison with untreated control cells.

Autofluorescence lifetime imaging of single cells became possible due to the availability of a novel picosecond laser diode with $\lambda = 375$ nm, which (in contrast to picosecond light sources above 400 nm) excites the coenzyme NADH efficiently. Extensive two-photon femtosecond laser systems [19,21] or Q-switched neodymium:YAG lasers, whose pulse duration is of the same order of magnitude as the fluorescence lifetimes of NADH [8,17], may thus be replaced by this kind of laser diode. A present limitation is the rather low pulse energy (≤ 5 pJ) corresponding to an average power lower than 200 μW when operated at 40 MHz. In addition, the light power is further reduced by diverse optical components (e.g. single mode fibers or microscope optics). Thus, a microscope objective lens of high numerical aperture (1.30) and moderate magnification (40$\times$) was needed in order to collect enough fluorescence photons for lifetime imaging. Spatial resolution was limited by the image intensifier to 320×240 pixels which corresponded to the pixel resolution of the CCD camera after 2×2 binning. For an image size of 320 μm $\times$ 250 μm, as depicted in Fig. 3, a spatial resolution of 1.0 μm was thus attained. This implies that the theoretical resolution of the objective lens given by $\Delta x = 0.61\lambda/A$ (with λ corresponding to the wavelength and A to the numerical aperture) could not be used, so far. Ultraviolet laser diodes emitting light pulses with higher power will permit the use of objective lenses of higher magnification in the near future. Therefore, the resolution given by the image intensifier (e.g. 0.4 μm for a 100$\times$ magnification lens) will approximate the theoretical value. In addition, high power laser diodes will open up a large field of applications, e.g. in time-resolved fluorescence endoscopy. The present measurements may be considered as a first step towards that direction.

ACKNOWLEDGMENT

REFERENCES

1. M. H. Gschwend, R. Rüdel, W. S. L. Strauss, R. Sailer, H. Brinkmeier, and H. Schneckenburger (2001). Optical detection of mitochondrial NADH content in human myotubes. *Cell. Mol. Biol.* **47**, OL95–OL104.
2. K. A. Horvath, K. T. Shomacker, C. C. Lee, and L. H. Cohn (1994). Intraoperative myocardial ischemia detection with laser-induced fluoroescence. *J. Thorac. Cardiovasc. Surg.* **107**, 220–225.
3. E. T. Obi-Tabot, L. M. Hanrahan, R. Cachecho, E. R. Beer, S. R. Hopkins, J. C. Chan, J. M. Shapiro, and W. W. LaMorte (1993). Changes in hepatocyte NADH fluorescence during prolonged hypoxia. *J. Surg. Res.* **55**, 575–580.
4. W. Lohmann and E. Paul (1988). In situ detection of melanomas by fluorescence measurements. *Naturwissenschaften* **75**, 201–202.
5. M. Anidjar, O. Cussenot, S. Avriller, D. Ettori, J. M. Villette, J. Fiet, P. Teillao, A. Le Duc (1996). Ultraviolet laser-induced fluorescence distinction between malignant and normal urothelial cells and tissues. *J. Biomed. Opt.* **1**, 335–341.
6. G. A. Wagnières, M. S. Willem, and B. C. Wilson (1998). In vivo fluorescence spectroscopy and imaging for oncological applications. *Photochem. Photobiol.* **68**, 603–632.
7. A. C. Croce, A. Spano, D. Locatelli, S. Barni, L. Sciola, and G. Bottiroli (1999). Dependence of fibroblast autofluorescence properties on normal and transformed conditions. Role of the metabolic activity. *Photochem. Photobiol.* **69**, 364–374.
8. A. Colasanti, A. Kisslinger, G. Fabbrocini, R. Liuzzi, M. Quarto, P. Riccic, G. Roberti, and F. Villani (2000). MS-2 fibrosarcoma characterization by laser induced autofluorescence. *Lasers Surg. Med.* **26**, 441–448.
9. L. Rigacci, R. Alterini, P. A. Bernabei, P. R. Ferrini, G. Agati, F. Fusi, and M. Monici (2000). Multispectral imaging autofluoroescence microscopy for the analysis of lymph-node tissues. *Photochem. Photobiol.* **71**, 737–742.
10. S. Andersson-Engels, J. Johansson, J. K. Svanberg, and S. Svanberg (1991). Fluorescence imaging and joint measurements of tissues: Applications to the demarcation of malignant tumors and atherosclerotic lesions from normal tissue. *Photochem. Photobiol.* **53**, 807–814.
11. T. Galeotti, G. D. V. VanRossum, D. H. Mayer, and B. Chance (1970). On the fluorescence of NAD(P)H in whole cell preparations of tumours and normal tissues. *Eur. J. Biochem.* **17**, 485–496.

12. J.-M. Salmon, E. Kohen, P. Viallet, J. G. Hirschberg, A. W. Wouters, C. Kohen, and B. Thoroll (1982). Microspectrofluorometric approach to the study of free/bound NAD(P)H ratio as metabolic indicator in various cell types. *Photochem. Photobiol.* **36**, 585–593.

13. M. Wakita, G. Nishimura, and M. Tamura (1995). Some characteristics of the fluorescence lifetime of reduced pyridine nucleotides in isolated mitochondria, isolated hepatocytes and perfused rat liver in situ. *J. Biochem.* **118**, 1151–1160.

14. T. G. Scott, R. D. Spencer, N. J. Leonard, and G. Weber (1970). Emission properties of NADH. Studies of fluorescence lifetimes and quantum efficiencies of NADH, AcPyADH, and simplified synthetic models. *J. Am. Chem. Soc.* **92**, 687–695.

15. H. Schneckenburger, M. H. Gschwend, W. S. L. Strauss, R. Sailer, M. Kron, U. Steeb, and R. Steiner (1997). Energy transfer spectroscopy for measuring mitochondrial metabolism in living cells. *Photochem. Photobiol.* **66**, 34–41.

16. R.-J. Paul and H. Schneckenburger (1996). Oxygen concentration and the oxidation-reduction state of yeast: Determination of free/bound NADH and flavins by time-resolved spectroscopy. *Naturwissenschaften* **82**, 32–35.

17. H. Schneckenburger, M. H. Gschwend, R. Sailer, H.-P. Mock, and W. S. L. Strauss (1998). Time-gated fluorescence microscopy in molecular and cellular biology. *Cell. Mol. Biol.* **44**, 795–805.

18. J. R. Lakowicz, H. Szmacinski, K. Nowaczyk, and M. L. Johnson (1992). Fluorescence lifetime imaging of free and protein-bound NADH. *Proc. Natl. Acad. Sci. U.S.A.* **89**, 1271–1275.

19. K. König, P. T. So, B. J. Tromberg, and E. Gratton (1996). Two-photon excited lifetime imaging of autofluorescence in cells during UVA and NIR photostress. *J. Microsc.* **183**, 197–204.

20. M. J. Cole, J. Siegel, S. E. Webb, R. Jones, K. Dowling, M. J. Dayel, D. Parsons-Karavassilis, P. M. French, M. J. Lever, L. O. Sucharov, M. A. Neil, R. Juskaitis, and T. Wilson (2001). Time-domain whole-field fluorescence lifetime imaging with optical sectioning. *J. Microsc.* **203**, 246–257.

21. K. König and I. Riemann (2003). High-resolution multiophoton tomography of human skin with subcellular spatial resolution and picosecond time resolution. *J. Biomed. Opt.* **8**(3), 432–439.

22. H. Schneckenburger, K. Stock, M. Lyttek, W. S. L. Strauss, and R. Sailer (2004). Fluorescence lifetime imaging (FLIM) of rhodamine 123 in living cells. *Photochem. Photobiol. Sci.* **3**, 127–131.

23. W. Halle, W.-E. Siems, K. D. Jentzsch, E. Teuscher, and E. Görres (1984). Die in vitro kultivierte Aorten-Endothelzelle in der Wirkstofforschung-Zellphysiologische Charakterisierung und Einsatzmöglichkeiten der Zellinie BKEz-7. *Die Pharmazie* **39**, 77–81.

24. A. Tzagaloff (1982). *Mitochondria*, Plenum, New York.

25. E. P. Buurman, R. Sanders, A. Draijer, H. C. Gerritsen, J. J. F. van Veen, P. M. Houpt, and Y. K. Levine (1992). Fluorescence lifetime imaging using a confocal laser scanning microscope. *Scanning* **14**, 155–159.

26. B. Chance (1976). Pyridine nucleotide as an indicator of the oxygen requirements for energy-linked functions of Mitochondria. *Circ. Res.* (Suppl.) 138 I-31–I-38.